

RESEARCH ARTICLE

MamA as a Model Protein for Structure-Based Insight into the Evolutionary Origins of Magnetotactic Bacteria

Natalie Zeytuni¹✉, Samuel Cronin¹✉, Christopher T. Lefèvre², Pascal Arnoux², Dror Baran¹, Zvi Shtein¹, Geula Davidov¹, Raz Zarivach^{1*}

1 Department of Life Sciences and The National Institute for Biotechnology in the Negev, Ben-Gurion University of the Negev, Beer Sheva, Israel, **2** CEA/CNRS/Aix-Marseille Université, UMR 7265 Biologie Végétale et Microbiologie Environnementales, Laboratoire de Bioénergétique Cellulaire, Saint Paul les Durance, France

✉ These authors contributed equally to this work.

* zarivach@bgu.ac.il



CrossMark
click for updates

Abstract

MamA is a highly conserved protein found in magnetotactic bacteria (MTB), a diverse group of prokaryotes capable of navigating according to magnetic fields – an ability known as magnetotaxis. Questions surround the acquisition of this magnetic navigation ability; namely, whether it arose through horizontal or vertical gene transfer. Though its exact function is unknown, MamA surrounds the magnetosome, the magnetic organelle embedding a biomineralised nanoparticle and responsible for magnetotaxis. Several structures for MamA from a variety of species have been determined and show a high degree of structural similarity. By determining the structure of MamA from *Desulfovibrio magneticus* RS-1 using X-ray crystallography, we have opened up the structure-sequence landscape. As such, this allows us to perform structural- and phylogenetic-based analyses using a variety of previously determined MamA from a diverse range of MTB species across various phylogenetic groups. We found that MamA has remained remarkably constant throughout evolution with minimal change between different taxa despite sequence variations. These findings, coupled with the generation of phylogenetic trees using both amino acid sequences and 16S rRNA, indicate that magnetotaxis likely did not spread via horizontal gene transfer and instead has a significantly earlier, primordial origin.

OPEN ACCESS

Citation: Zeytuni N, Cronin S, Lefèvre CT, Arnoux P, Baran D, Shtein Z, et al. (2015) MamA as a Model Protein for Structure-Based Insight into the Evolutionary Origins of Magnetotactic Bacteria. PLoS ONE 10(6): e0130394. doi:10.1371/journal.pone.0130394

Editor: John R. Battista, Louisiana State University and A & M College, UNITED STATES

Received: March 2, 2015

Accepted: May 20, 2015

Published: June 26, 2015

Copyright: © 2015 Zeytuni et al. This is an open access article distributed under the terms of the [Creative Commons Attribution License](https://creativecommons.org/licenses/by/4.0/), which permits unrestricted use, distribution, and reproduction in any medium, provided the original author and source are credited.

Data Availability Statement: All relevant data are within the paper and its Supporting Information files.

Funding: This research was made possible through grants from the Israeli Ministry of Science, Technology and Space and EMBO, the European Molecular Biology Organisation.

Competing Interests: The authors have declared that no competing interests exist.

Introduction

Magnetotactic bacteria (MTB) are a diverse group of prokaryotes capable of movement according to magnetic fields—an ability known as magnetotaxis. This characteristic is believed to have developed to enable these aerobic or anaerobic, aquatic, Gram negative bacteria to optimally find the oxic-anoxic boundary [1]. This is achieved via the internal biomineralisation of magnetic nanoparticles of either magnetite (Fe₃O₄) or greigite (Fe₃S₄) by a specific organelle, the

magnetosome. Each of these membrane-bound organelles biomineralises a single magnetic crystal, following which the organelles are aligned into a chain, creating a magnetic moment [2].

First brought to wide scientific attention in 1975, approximately 30 species of MTB have been studied and their genomes sequenced [3,4]. Until the early 90s, it was thought that MTB were restricted to the *Alphaproteobacteria* class. With the discovery of the multicellular magnetotactic prokaryotes [5] and *Desulfovibrio magneticus* strain RS-1 [6] the diversity of MTB extended to the *Deltaproteobacteria* class. Later, magnetotactic bacteria were found in three other major groups of the prokaryotes: the *Nitrospirae* [7], the *Gammaproteobacteria* class [8] and the OP3 division [9]. *Desulfovibrio magneticus* RS-1, which shares 98.7% similarity of its 16S rRNA gene sequence with *Desulfovibrio burkinensis*, is a magnetite-containing microorganism related to dissimilatory sulphate-reducing bacteria [10].

Many of the magnetosome-associated genes are found on a highly conserved genomic cluster known as the *magnetosome island* [1]. In particular, the protein MamA is highly conserved amongst MTB [11]. Considerable research has focused on the origins of magnetotaxis; that is, whether there is a monophyletic origin for this ability or whether it was acquired through horizontal gene transfer (HGT) [12,13]. Of the magnetosome genes, studies have found these either to be essential, in that deletion results in a noticeable change or loss of function, or inessential; research has found that these inessential genes are easily lost during magnetosome evolution. MamA, on the other hand, unexpectedly is neither—deletion of the *mamA* genes results in no significant change in function in cultivated cells, yet MamA is almost perfectly conserved and is rarely lost [14,15]. Indeed, *mamA* belongs to the nine “core genes” essential for magnetosome formation [16,17], though it has yet to be determined specifically how it is essential. *Nitrospirae* and *Deltaproteobacteria* represent two of the most deeply branching groups of MTB and, along with the *Alphaproteobacteria*, all of these MTB carry in their genome a copy of *mamA*; this protein is therefore a prime candidate for comparative structural studies determining protein conservation between different, distantly related species, as well as for attempting to illuminate on the origins of MTB.

The hypothesis for the earlier, primordial development of magnetotaxis—as opposed to its acquisition via HGT—is further supported by the physical shape of the magnetic nanocrystals; the magnetosomes of *D. magneticus* RS-1 (hereafter, RS-1) synthesise anisotropic, bullet-shaped magnetite particles, similar to those produced by the known MTB of the *Nitrospirae*, “*Candidatus Magnetobacterium bavaricum*”, (hereafter, Mbav). Conversely, MTB of the much later-diverging *Alpha*- and *Gammaproteobacteria* will only produce well-defined, cuboctahedral crystals [13].

MamA is a magnetosome-associated protein (MAP) involved in the biomineralisation process by coating the magnetosome membrane [18]. It has previously been genetically manipulated and the structures of its $\Delta 41$ mutants—created by removing the putative N-terminal TPR repeat—solved in multiple species of MTB, mostly *Alphaproteobacteria* (*Magnetospirillum magneticum* AMB-1, PDB code: 3AS5; *Magnetospirillum gryphiswaldense* MSR-1, PDB code: 3AS8; and Mbav, PDB code: 3VTX) [11,19]. This 23 kDa protein is comprised of five tetratricopeptide repeats (TPR), a 34 amino acid structural motif. Each TPR consists of a helix-turn-helix fold, in addition to a putative N-terminal repeat. As such, MamA adopts an overall superhelical structure enabling the protein to be highly involved in protein-protein interactions via two main binding sites, one at its concave surface and the other at its convex surface [19].

Studies have been performed using MamA from Mbav (from the *Nitrospirae* phylum) and from the *Magnetospirillum* genus, which represent the evolutionary/phylogenetic ends of MTB; by choosing RS-1 as our model organism we provide here a full spread across the evolutionary landscape, with a magnetotactic *Deltaproteobacteria* between the two extremes. Here,

we have solved a new structure for MamA from the alternative species, *Desulfovibrio magneticus* strain RS-1, and compare between other, previously solved MamA structures and this distantly related species of MTB. Comparative structural analysis gives an insight into the evolution of magnetotaxis.

Results and Discussion

MamA Δ 41 purification and crystallisation

To obtain biochemical and structural information toward comparative studies, recombinant MamA Δ 41_{RS-1} was overexpressed in *Escherichia coli* cells. MamA Δ 41_{RS-1} was found to be soluble and stable in a buffer solution containing high NaCl concentration (> 0.5 M), whereas previously characterised MamA Δ 41 from different species were soluble at lower NaCl concentrations (~150 mM) [11,19–21]. Size-exclusion chromatography revealed that MamA Δ 41_{RS-1} elutes at a volume that corresponds to an octamer, whilst MamA Δ 41 proteins from different species were found as either trimers or monomers (S1 Fig). The purified MamA Δ 41_{RS-1} was subjected to numerous crystallisation trials using a sitting drop vapour diffusion methodology. Those crystallisation trails did not result in any crystal nucleation, even after subjecting the protein to lysine methylation and limited proteolysis. To overcome this crystallisation obstacle we utilised Surface Entropy Reduction (SER), which suggests replacing surface-exposed high entropy amino acids with residues that have small, low entropy side chains, such as alanines. Residues of particular importance are lysines and glutamates as statistical analyses show that both are localised predominantly on the surface [22] and are disfavoured at protein-protein interfaces [23]. We submitted the MamA Δ 41_{RS-1} protein sequence to the SERp web-server (<http://services.mbi.ucla.edu/SER/>) [24] and followed its suggestion to mutate three surface predicted residues—Glu140, Lys141 and Glu143—to alanines. As such, the triple mutated protein, named MamA Δ 41 RS-1 TM (henceforth, ArSTM), was overexpressed and purified in the same manner as the wild-type MamA Δ 41_{RS-1}. The size-exclusion chromatography elution profile of ArSTM displayed some differences in reference to MamA Δ 41_{RS-1}, as the mutated protein eluted at three distinct volumes. By comparing these volumes to a standard calibration curve we determined that the three peaks correspond to sizes of a 13-meric oligomer, an octamer and a monomer (S1 Fig). Crystallisation trials of octameric and monomeric ArSTM resulted in the appearance of a single crystal form that diffracted to a resolution of 2.88 Å (see Table 1 for data collection and refinement statistics). Phase information was obtained by the molecular replacement technique and, after rounds of manual rebuilding and refinement, we obtained a high quality structure (Table 1) with almost a full cover of the protein sequence (S1 Table).

Phylogenetic analyses of MamA

MamA protein can be retrieved from 30 known MTB genomes. A total of 32 sequences could be found due to the presence of two copies of *mamA* in strains HK-1 [9] and BW-1 [17] that appear to have two clusters of *mam* genes, one for magnetite and the other for greigite magnetosome formation. All 32 MamA proteins contain five TPR domains except for strains UT-2, UT-4, LEMS, NML-1, SS-4, KR-1, CB-1, CC-2, LM-5, LM-2 and UT-1 whose C-terminal extremity remains incompletely sequenced. Using principal component analysis, we could not find a relation between the five TPR motifs that appear to have evolved from a common MamA-like ancestor that originally had the five TPR motifs (data not shown), rather than an evolution where one original TPR would have duplicated to give rise to the other TPR motifs. Although all 32 MamA proteins presumably have the same function in the different MTB based on their presence and synteny conservation in the *mamAB* operon between the different MTB from the different phylogenetic group, at first glance a BLAST search of a MamA does

Table 1. Crystallographic data for ARS_{TM}.

PDB code Protein	4X10 MamAΔ41
Data collection	ID14-4 - ESRF
Space group	I ₄
Cell dimensions	
a, b, c (Å)	151.087, 151.087, 204.903
α, β, γ (°)	90, 90, 90
Resolution (Å)	2.88
R _{sym} or R _{merge}	6.5 (60.8)
I / σ	43.89 (3.64)
Completeness (%)	99.8 (100)
Redundancy	6.2
Wavelength (Å)	0.939
Refinement	
Resolution (Å)	2.88
No. reflections	51648
R _{work} / R _{free}	20.94/22.01
No. atoms	
Protein	8530
Ligand/ion	
Water	
B-factors	
Protein	77.52
Ligand/ion	
Water	
R.m.s. deviations	
Bond lengths (Å)	0.0237
Bond angles (°)	1.8972

doi:10.1371/journal.pone.0130394.t001

not retrieve the homologous proteins from MamA that are phylogenetically distant. For instance, MamA from magnetotactic *Alphaproteobacteria* are too divergent from the MamA of the magnetotactic *Deltaproteobacteria* (e.g. MamA of strain AMB-1 having only 24% identity with MamA of strain RS-1). Thus, although MamA appears to be well conserved in all MTB based on domain conservation, only a precise comparative genomic analysis allows finding homologues in other phylogenetically distant genomes.

We aligned the MamA amino acid sequences from the 21 complete MamA proteins (S2 Fig). Phylogenetic trees based on MamA amino acid sequences and 16S rRNA gene sequences show a congruency and a conservation of the different groups that contain MTB (Fig 1). This indicates that *mamA* evolved monophyletically, like the others magnetosome genes, from a common ancestor of all MTB.

These findings are reinforced by analysis using ConSurf [25,26], a tool for determining evolutionary conservation of amino acids using phylogenetics, which displayed a high degree of structural conservation between ARS_{TM} and MamA from other species of MTB (Fig 2). In particular, the fifth TPR around the C-terminus is highly conserved, as well as the concave surface of the protein. Conversely, the backbone of the monomer is distinctly unconserved displaying only a few small conserved patches that are clusters of single or double residues.

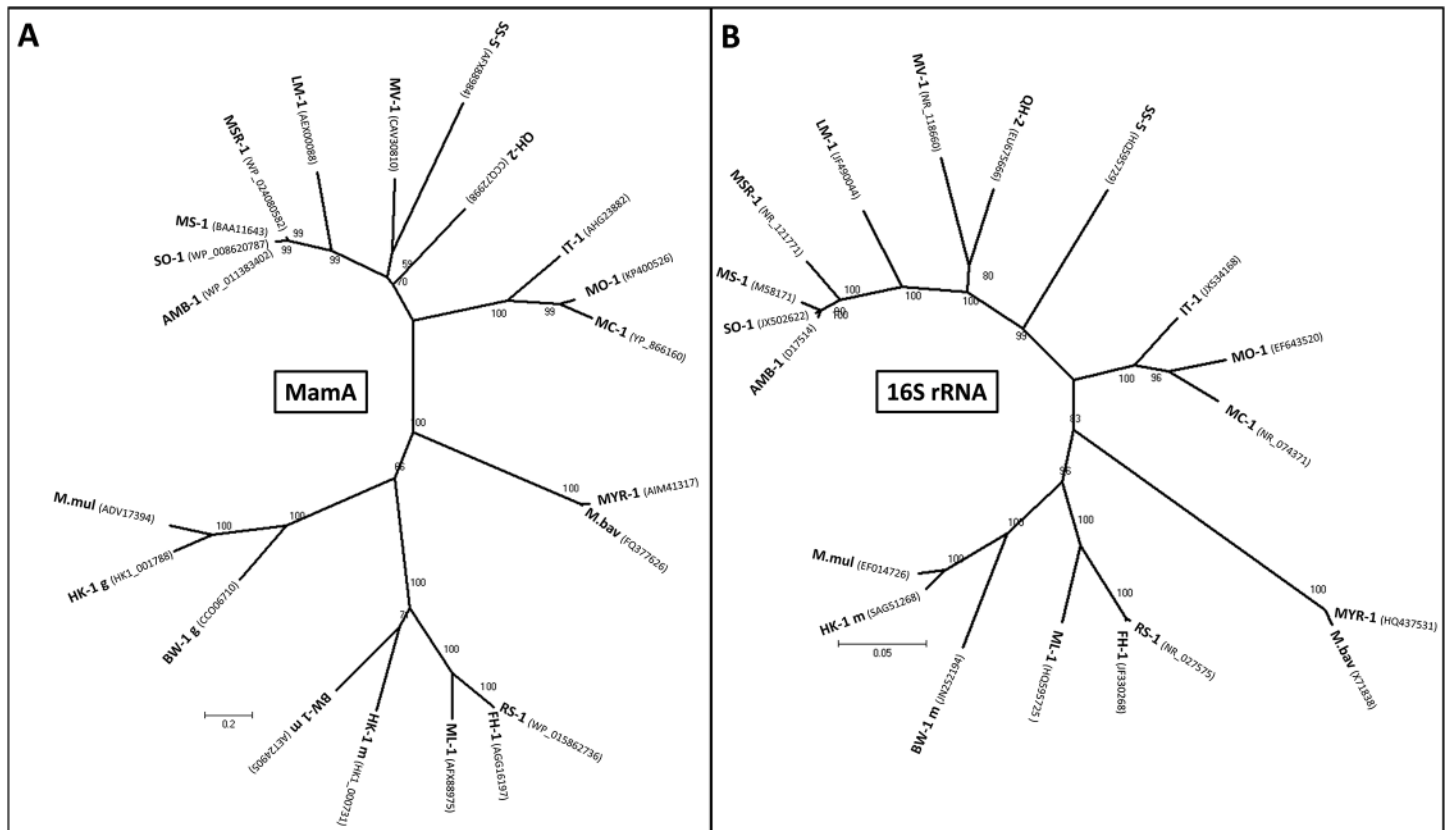


Fig 1. Congruency of the phylogenetic trees based on (A) MamA protein sequences and on (B) 16S rRNA gene sequences that reflect the evolution of MTB. Scale bars represent the percentage sequence divergence. Bootstrap values at nodes are percentages of 100 replicates. The MTB from *Alphaproteobacteria* class used in the analyses are: *Magnetospirillum magnetotacticum* (strain MS-1), *Ms. magneticum* (AMB-1), *Ms. gryphiswaldense* (MSR-1), strain SO-1, strain LM-1, *Magnetovibrio blakemorei* (MV-1), *Magnetospira* sp. QH-2, strain MO-1, *Magnetofaba australis* (IT-1) and *Magnetococcus marinus* (MC-1). Strain SS-5 from the *Gammaproteobacteria* class is also used. From the *Deltaproteobacteria* class MTB used include the magnetotactic multicellular prokaryotes *Ca. Magnetoglobus multicellularis* (MMP) and strain HK-1, *Ca. Desulfamplus magnetomortis* (BW-1), *Desulfovibrio magneticus* (RS-1 and FH-1), and strain ML-1. *Ca. Magnetobacterium bavaricum* (Mbav) and strain MYR-1 of the *Nitrospirae* phylum was also used. Accession numbers are shown in parenthesis.

doi:10.1371/journal.pone.0130394.g001

ArSTM crystal packing

ArSTM monomers assemble to form a trimeric ring, each enclosing a ~15 Å diameter inner void (Fig 3A); the crystal asymmetric unit includes six ArSTM monomers arranged as two trimeric rings (Fig 4A). The employed forces that allow the stabilisation of each trimeric ring include salt bridges as well as hydrophobic interactions between the N-terminal of a single monomer and the C-terminal of a nearby monomer in a continuous manner, resulting in a ring with surface properties akin to a Möbius strip. These ring-stabilising salt bridges include a double salt bridge between Glu61 and Tyr65 from a single monomer to Gln183 from the nearby monomer, as well as a single salt bridge between Arg56 from a single monomer to Glu209 from the nearby monomer. The network of hydrophobic interactions includes Lys42, Leu45, Tyr46, Ile49, Arg52, Ser53, Arg64 and Glu68 from the N-terminal of a single monomer to Phe187, Val190, Ala198, Ala199, Phe202, Val205 and Met206 to the C-terminal of the nearby monomer (Fig 3B). As such, ArSTM presents a distinctly atypical binding surface since, as mentioned, the protein-protein interactions involving MamA typically bind via the concave or convex surfaces. Overall, the trimeric ring contains three of these identical, N-to-C-terminal interaction surfaces. Unexpectedly, but not altogether unsurprisingly, the triple mutated

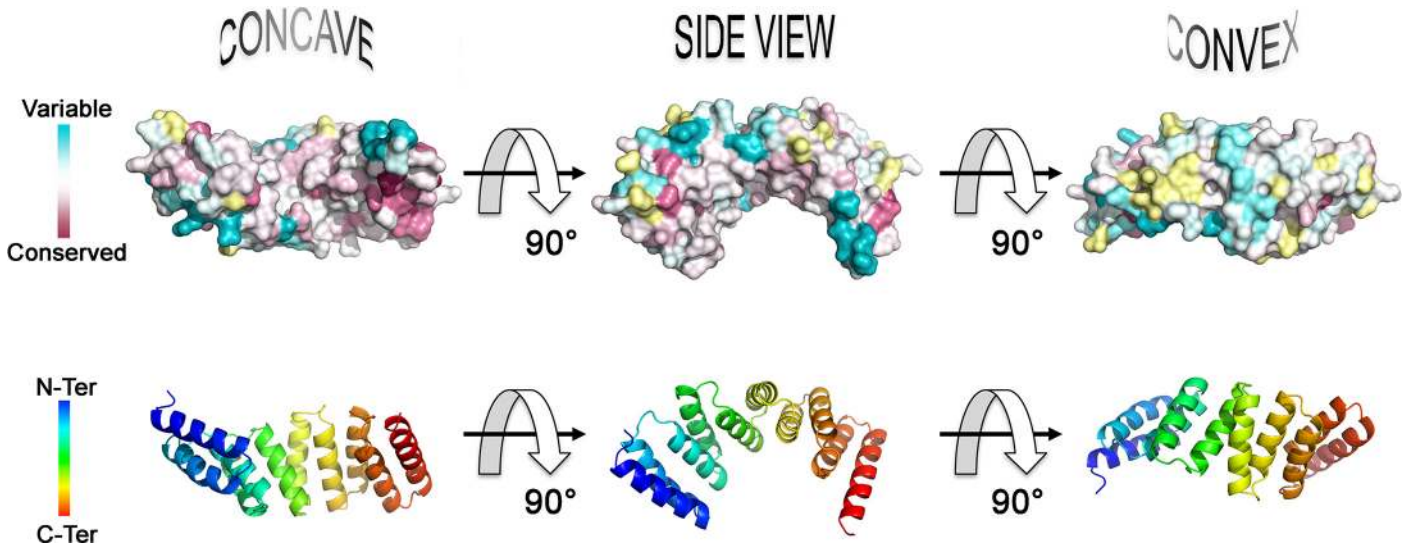


Fig 2. ConSurf analysis shows a high degree of structural conservation between Ar_STM and MamA from alternative species, though this is largely limited to the concave surface and a cluster around the fifth TPR and the C-terminal. All sequences used in this analysis are shown in the multiple sequence alignment of [S2 Fig](#).

doi:10.1371/journal.pone.0130394.g002

residues (E140A, K141A and E143A), along the ‘backbone’ of the monomers, were found to be at the centre of a crystal contact ([S3 Fig](#)). The tight packing of Ar_STM within the crystal could not occur with the original residues, which contained long and charged side chains and hence, could not be crystallised. This interaction surface includes two symmetric backbone polar contacts between two monomers (Phe111 to Ala140), where each monomer originates from a different ring. In addition, the interaction surface is stabilised through double hydrophobic interactions between Pro142 to His 110 ([S3 Fig](#)).

Ar_STM overall structure

The overall structure of the Ar_STM monomer contains 10 anti-parallel α -helices, folded as five TPR helix-turn-helix motifs, namely TPR1 (H1 and H2), TPR2 (H3 and H4), TPR3 (H5 and H6), TPR4 (H7 and H8) and TPR5 (H9 and H10), similar to previously determined MamA structures ([Fig 4B](#)). These TPR motifs give rise to a structure displaying concave and convex surfaces. All six Ar_STM monomers adopted the same overall fold, as the average root mean square deviation (RMSD) between the C α of the monomers ranges between 0.08–0.1 Å ([Fig 4B](#)). Additionally, we tested for the secondary structure of the protein in solution using circular dichroism (see below, *NTD stabilisation and the functionality of the conserved salt bridge*). Overall, all MamA variants are folded as alpha helices, as predicted for a TPR-containing protein. Our results show highly similar structures for Ar_STM, wild type MamA Δ 41 RS-1 and MamA from Mbav, indicating that our mutations had no alteration effect on the helices of MamA Δ 41 RS-1. Whilst MamA from both AMB-1 and MSR-1 display slight deviation from the other three MamA proteins, they all still remain highly similar. Overlapping Ar_STM on MamA structures from *Magnetospirillum magneticum* AMB-1, *Magnetospirillum gryphiswaldense* MSR-1 and Mbav also yielded low RMSD values ranging between 1.26–1.70 Å ([Fig 4C](#) and [S2 Table](#)) [11]. These low RMSD values together with the sequence conservation indicate that the MamA Δ 41 structure is conserved across phyla, which runs counter to the hypothesis of HGT.

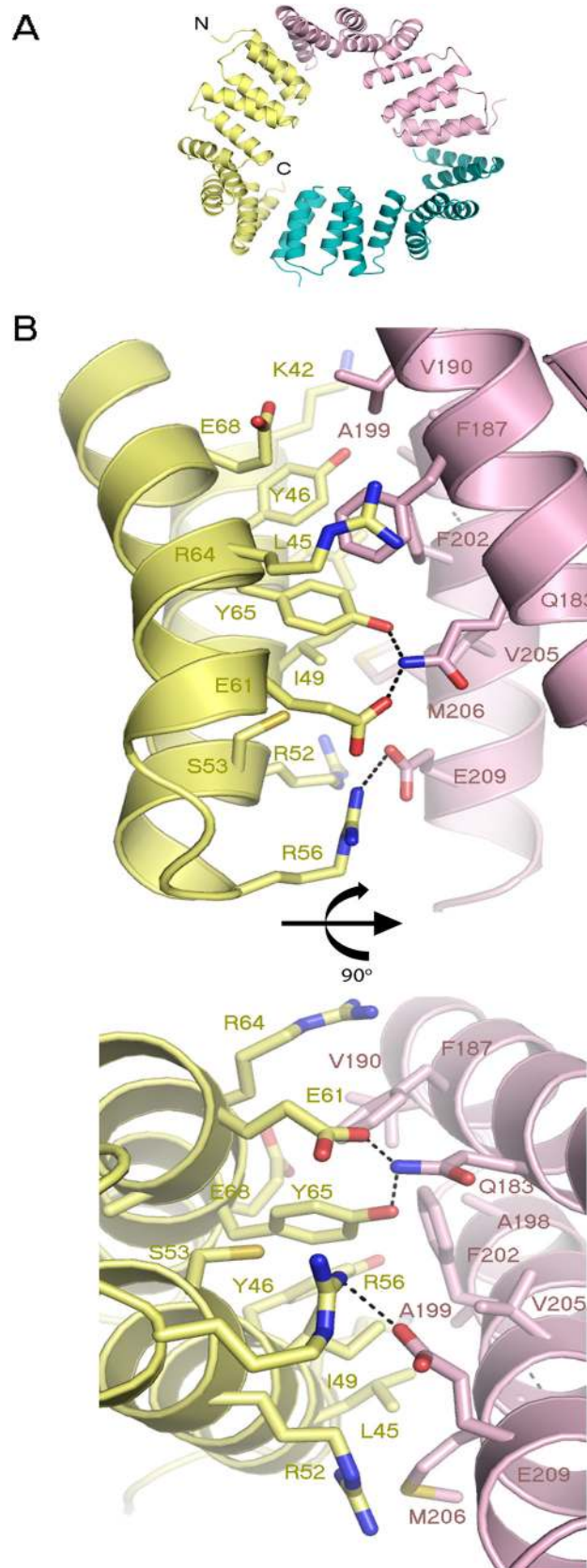


Fig 3. (A) Three ArsTM monomers form the trimeric ring. This flat ring encloses a ~15 Å diameter inner void. **(B)** Interaction surface between two monomers that form the trimeric ring. The forces that stabilise the trimeric ring include salt bridges as well as hydrophobic interactions between the N-terminal of a single monomer to the C-terminal of a nearby monomer in a continuous manner.

doi:10.1371/journal.pone.0130394.g003

Like MamA Δ 41 from *Magnetospirillum* and Mbav species, ArsTM also displays the typical electrostatic charge distribution, with its concave surface potential being mainly positive. However, the convex surface potential of ArsTM contains a mixture of positive and negative patches and thus is more similar to MamA Δ 41Mbav convex surface, while in *Magnetospirillum* species this region is mainly negative (S4 Fig).

Previously determined MamA Δ 41 structures from *Magnetospirillum* and Mbav species displayed a unique separation into two distinct domains [11]. The hinge region that separates between the N-terminal domain (NTD), which includes TPR motifs 1–2, and the C-terminal domain (CTD), which includes TPR motifs 3–5, is located at the loop connecting TPR2 to TPR3. This flexible hinge region allows a radial movement of the NTD in reference to the CTD upon binding of a putative ligand at the concave surface [11]. In ArsTM we could not detect such domain movement, as the conformations of all six monomers are similar. However, by overlapping ArsTM monomers onto the available MamA Δ 41 structures that did display such NTD movement, we could see that the curvature of ArsTM is more similar to the putative ligand binding conformation (i.e. MamA Δ 41_{AMB-1} PDB code: 3AS5 chain B, and MamA Δ 41_{Mbav} PDB code: 3VTX) (Fig 4C and S1 Table). Such curvature of ArsTM, though no putative ligand was observed at the crystal structure, could have been more favourable due to the trimeric rings' local packing as well as other crystal contacts.

The five-TPR set-up and its associated hinge region further separate MamA from other TPR-containing proteins; other TPR proteins generally possess either far fewer repeats (approximately three), to allow for domain separation, or far greater, resulting in a continuous superhelical structure, free of the kinked hinge region found in MamA. The high degree of sequence variation surrounding the structurally conserved hinge region indicates that there was sufficient time for this evolution to occur, counter to the structural- and sequence-homogeneity that would occur via HGT. That all thus-far described MamA proteins from various species possess these structural motifs resulting in the same, overall structure, unique among TPR proteins, further indicates for a single origin that has undergone evolutionary sequence changes over time but retained both its overall structural elements and its function within the various species of MTB.

Multiple sequence alignment between ArsTM and MamA from other species shows a distinct lack of conservation around the connecting loops between the helices, including the hinge region described above (S2 Fig). These regions are similar in the *Magnetospirillum* spp. MTB but there is significant variation for MamA from the deeply-branching RS-1 and “*Ca. M. bavaricum*”; we hypothesise this to be due to the loops not participating in any protein-protein interactions and thus there is no need for these to remain conserved.

NTD stabilisation and the functionality of the conserved salt bridge

MamA proteins from different species display a high degree of sequence and structural similarity (S2 Fig) [11,19]. Most of the fully conserved residues are related to the TPR motif consensus sequence apart from Asp159. Previous work on *Magnetospirillum* species revealed that mutating Asp159 had no effect on the overall structure of MamA Δ 41, MamA complex formation or the *in vivo* sub-cellular localisation to the magnetosome chain [19]. Nevertheless, it is possible that Asp159 mediates other cellular protein-protein interactions with MamA. In addition to

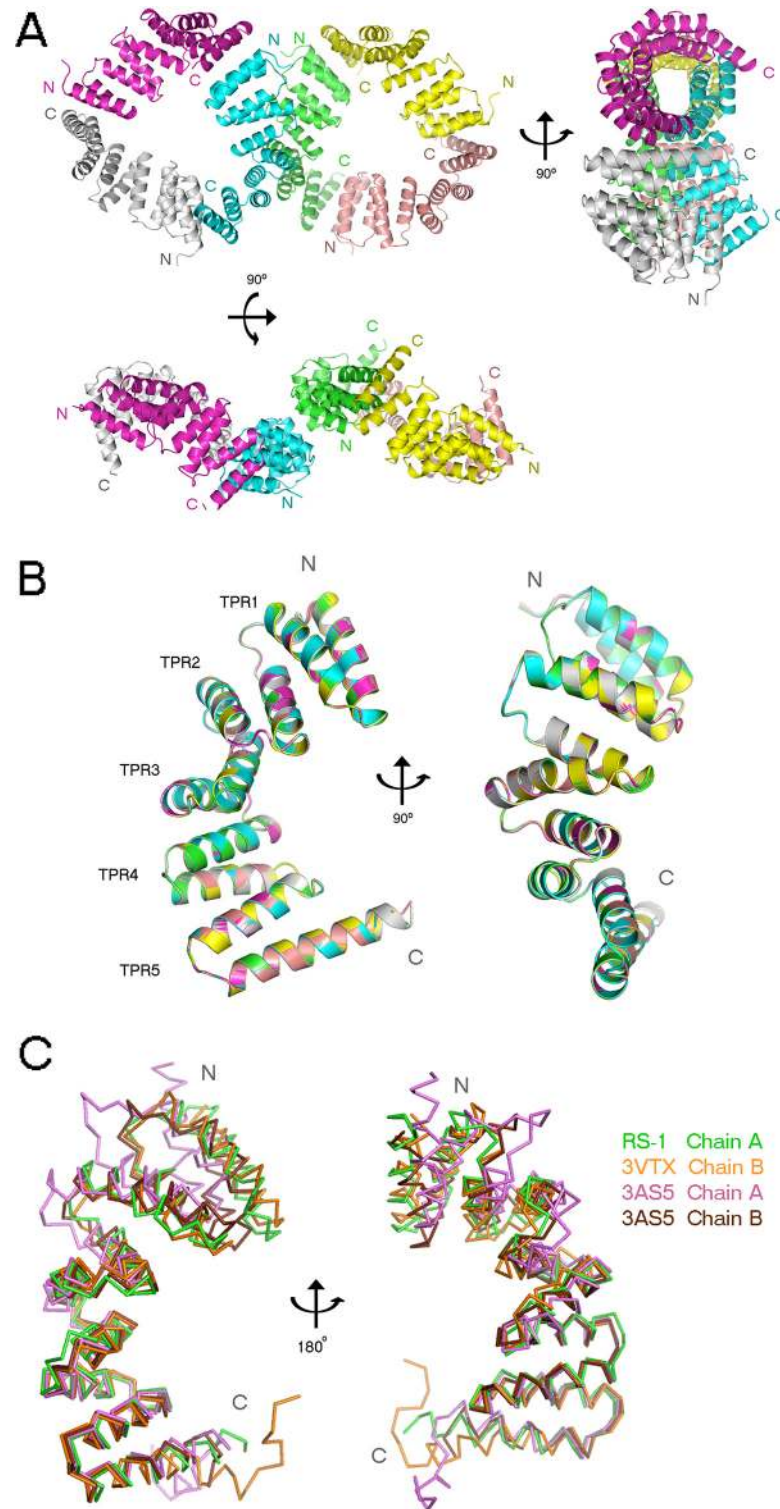


Fig 4. ARS-TM crystal packing, asymmetric unit composition and overall structure. (A) ARS-TM crystal packing and asymmetric unit composition. The molecules are shown in three rotation-related views. (B) Overlay of all six ARS-TM monomers reveals the high degree of structural similarity. The representative ARS-TM monomer contains five sequential TPR motifs. The molecule is shown in two views, related by a 90° rotation. (C) An overlay of representative monomers from ARS-TM (green), MamAΔ41_{Mbav} (PDB ID: 3VTX, orange) and *Magnetospirillum* species MamAΔ41_{AMB-1} (PDB ID: 3AS5 chain A and B in light pink and brown,

respectively) related by a 180° rotation. A high structural similarity of MamA Δ 41 between the species can be observed, apart from the helical conformation of the identical His-tag linker sequence remaining after thrombin proteolysis (H11: ELALVPR) seen in the 3AS5 chain B and 3VTX. In addition, a light flexibility is observed at the NTD of the monomers. All images were produced by PyMOL.

doi:10.1371/journal.pone.0130394.g004

Asp159, two other MamA residues, Arg50 and Asp79, were considered to be highly conserved in all available species prior to the release of Mbav and BW-1 (a magnetotactic *Deltaproteobacteria*) sequences. The determined structures of MamA from *Magnetospirillum* species revealed that Arg50 and Asp79 form a salt bridge that stabilises the NTD by connecting the TPR1 and TPR2 motifs. Whilst these salt bridge-forming residues are conserved in ARSTM (Arg47 and Asp76), the salt bridge itself is not since the distance between these two residues is too great (Fig 5A). Furthermore, due to steric interference by the large Trp69, clearly shown in the structure, we could find no rotameric combinations for Arg47 and Asp76 capable of forming the salt bridge around Trp69. Trp69 occupies a large volume and is part of an extensive hydrophobic surface that stabilises the NTD packing. We presume that, due to the large volume of the Trp69 side chain, motifs TPR1 and TPR2 cannot be packed as tightly as their homologous motifs from *Magnetospirillum* species and MamA Δ 41_{Mbav} (Fig 5B & 5C).

In other species, it has been found that disruption of this salt bridge altered the orientation of the NTD in relation to the CTD, eliminated the ability of MamA to homo-oligomerise and caused *in vivo* protein mislocalisation [19]. Despite having such a significant structural role, these conserved salt bridge-forming residues were altered in MamA sequences from Mbav and BW-1. An explanation for the remaining functionality of MamA Δ 41_{Mbav} NTD, although losing its conserved salt bridge, was previously suggested; namely that broad electrostatic interactions between the first two TPR motifs can compensate for the loss of this conserved salt bridge [11]. As such, evolution may have yielded a solution to the loss of the salt bridge whilst retaining the overall structure.

Despite Trp69 steric interference, we believe that the NTD domain of ARSTM remains stable due to the hydrophobic pi-pi stacking formed between Trp69 and Arg47. The overall interactions which stabilise the NTD of ARSTM are solely hydrophobic interactions and involve residues: Met39, Lys42, Arg47, Gln51, Leu54, Pro59, Leu63, Leu66, Trp69, Ala70, His72, Pro79, Gln83, Met83, Ala86 and Leu90 (Fig 5A). Such stabilisation through hydrophobic interactions is considered to be weaker than stabilisation through polar interaction and salt bridges, as observed in the NTDs of MamA Δ 41 from *Magnetospirillum* species and MamA Δ 41_{Mbav}. MamA Δ 41_{Mbav} presents the tightest and most stable interaction surface, stabilised by an extensive hydrogen bond network at the surface of TPR1 and TPR2, along with a salt bridge, and around the TPR2-3 connecting loop. A more moderate and intermediate stabilisation pattern can be seen in MamA Δ 41 from *Magnetospirillum* species, which presents a mixture of salt bridge, polar and hydrophobic interactions. ARSTM, on the other hand, lacks the stabilising network of hydrogen bonds but displays tight packing between TPR1 and TPR2, achieved mainly by a hydrophobic interaction network (Fig 5A).

The described variations between stabilisation patterns of the NTD among MamA proteins from different species can be linked to the overall thermostability seen in circular dichroism spectrometry. Melting temperature measurements revealed that MamA Δ 41_{RS-1} presents a reduced thermostability, with a melting temperature of 45°C, while MamA Δ 41_{AMB-1}, MamA Δ 41_{MSR-1} and MamA Δ 41_{Mbav} present melting temperatures of 51, 53 and 65°C, respectively (Fig 6). The most thermostable protein is MamA Δ 41_{Mbav}, which employs only polar interactions to stabilise its NTD, whereas the least thermostable protein is MamA Δ 41_{RS-1}, which employs only hydrophobic interactions. In between this thermostability range we can

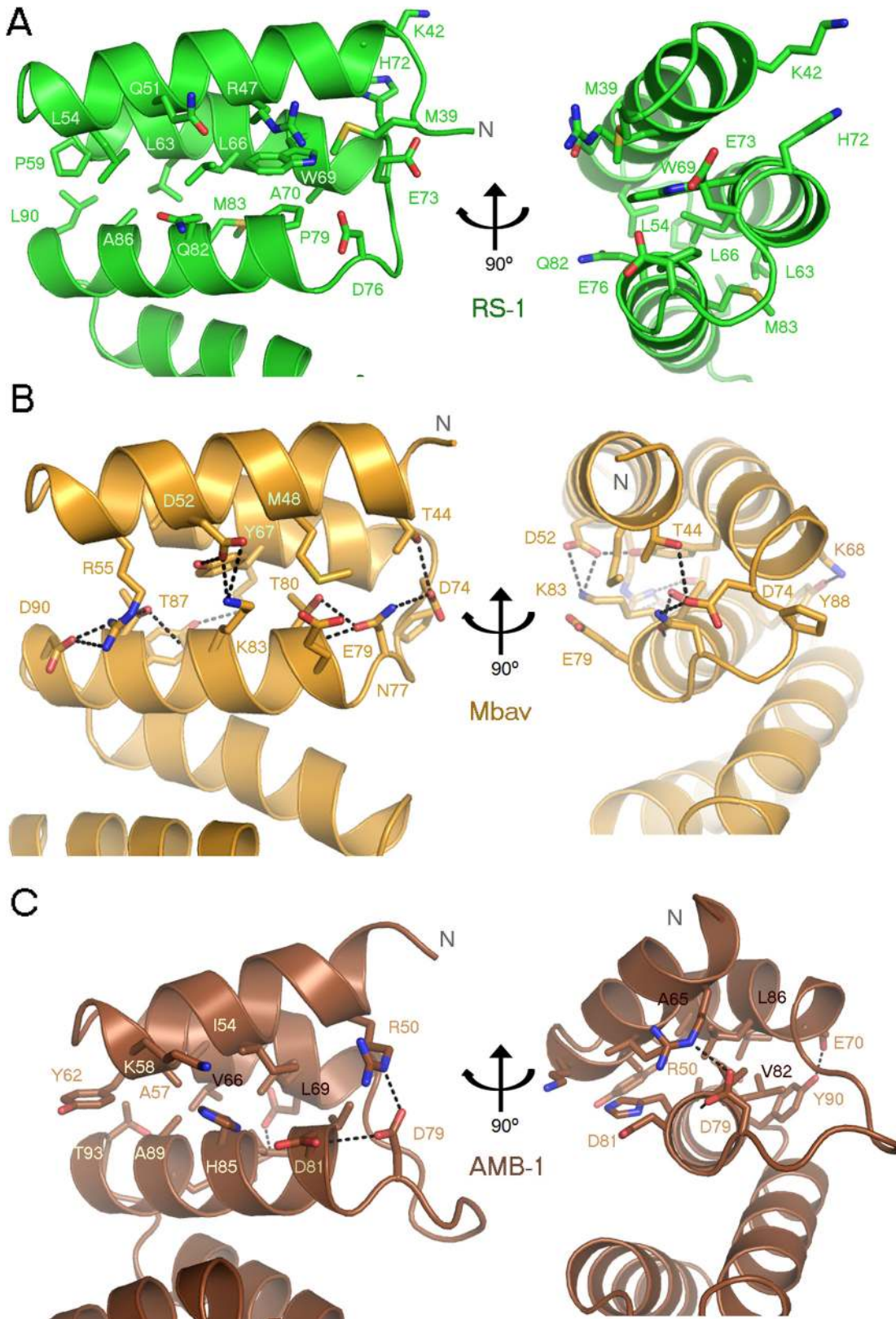


Fig 5. NTD stabilisation of MamA Δ 41 from different species. (A) Detailed representation of the interactions stabilising the ArS TM NTD. The ArS TM NTD is stabilised by a diverse network of hydrophobic interactions. (B) Detailed representation of the interactions stabilising the MamA Δ 41_{Mbav} NTD. The

MamA $\Delta 41_{Mbav}$ NTD is stabilised by a diverse network of hydrogen bonds and a single non-conserved salt bridge. **(C)** Detailed representation of the interactions stabilising the MamA $\Delta 41_{AMB-1}$ NTD. The MamA $\Delta 41_{AMB-1}$ NTD is stabilised through numerous hydrophobic interactions, a few hydrogen bonds and a single conserved salt bridge. Both NTD domains are shown in two views, related by a 90° rotation.

doi:10.1371/journal.pone.0130394.g005

find MamA $\Delta 41$ from *Magnetospirillum* species, which employ both types of interactions. We could also see that subjecting MamA $\Delta 41_{RS-1}$ to the triple surface entropy reduction mutations increased its thermostability by 6°C, by which it reached the same temperature as MamA $\Delta 41_{AMB-1}$. In order to obtain coherent and comparable results, we examined the octameric forms for both MamA $\Delta 41_{RS-1}$ and ArsTM during the circular dichroism spectrometry measurements. Accordingly, we believe that such slightly increased thermostability is due to the increased structural stability between ArsTM monomers when assembled as oligomers in solution (S1 Fig).

Conclusion

Our studies reveal that the structure of MamA has remained remarkably conserved throughout evolution with minimal change across different taxa. In particular, there is a high degree of structural conservation for the hinge region, CTD and NTD, indicative for a similar–yet unknown–function for MamA in all MTB, despite sequence variations. As such, MamA may be the most structurally conserved magnetosome-associated protein. This structural conservation is not limited to a particular motif but runs throughout the entire structure, from the five-TPR superhelical structure through to the hinge region. Our data enabled us to create evolutionary trees for MamA based on the amino acid sequences as well as on the 16S rRNA. A comprehensive approach to these data, together with the sequence variation and solutions to maintain the structural effects of the salt bridge, indicates that magnetotaxis likely did not spread via horizontal gene transfer and instead has a significantly earlier, primordial origin.

Materials and Methods

Protein Expression and Purification

Both full length and truncated MamA were amplified by whole-cell polymerase chain reaction (PCR) from *Desulfovibrio magneticus* RS-1 (kindly provided by Prof. Arash Komeili, Berkley,

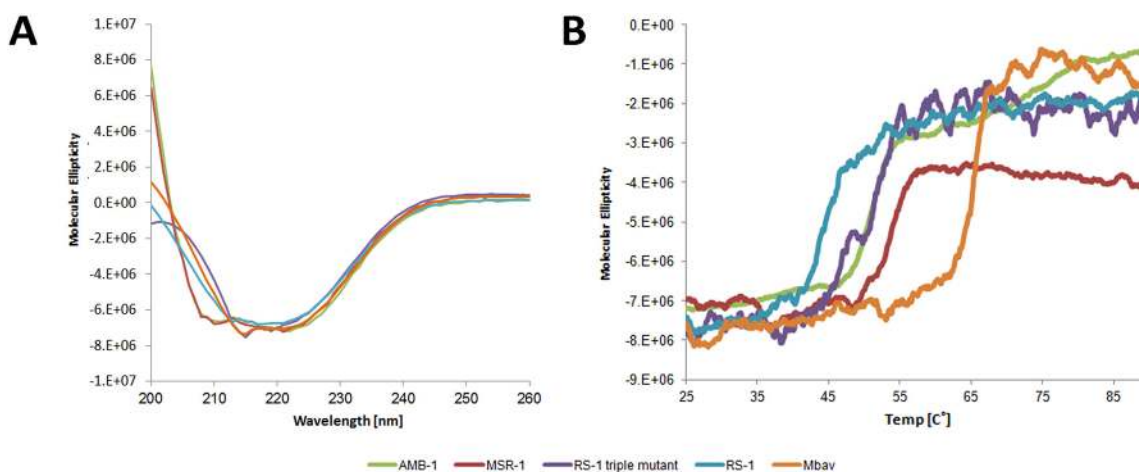


Fig 6. Circular dichroism measurements of ArsTM (purple) and MamA $\Delta 41$ proteins from RS-1 (Blue) Mbav (orange), AMB-1 (green) and MSR-1 (red). (A) Circular dichroism spectra. (B) Circular dichroism melting curve measurements at 222 nm. Wild type MamA $\Delta 41_{RS-1}$ presents the lowest thermostability, with a melting temperature of ~40°C, while the triple mutated MamA $\Delta 41_{RS-1}$ (ArsTM) exhibits a slightly increased thermostability with a melting temperature of ~51°C. MamA $\Delta 41_{AMB-1}$, MamA $\Delta 41_{MSR-1}$ and MamA $\Delta 41_{Mbav}$ present melting temperatures of ~51, 53 and 65°C, respectively.

doi:10.1371/journal.pone.0130394.g006

California, USA). Amplified products contained an inserted N-terminal NcoI restriction site followed by a glycine codon (GGA) in order to maintain reading frame and a C-terminal SacI restriction site eliminating the gene's normal stop codon. Amplified products were recovered, digested and ligated into pET52(b) expression vector (Novagen) containing a C-terminal histidine₁₀ tag. An additional, seemingly silent, spontaneous mutation was discovered during gene sequencing at residue M124I. Transformed *E. coli* Rosetta strain cells were cultivated in auto-induction medium [27] containing ampicillin and chloramphenicol (100 mg ml⁻¹ and 30 mg ml⁻¹ respectively). Cultivated cells were kept at 310 K for 6 hours and then at 300 K for an additional 60 hours. Cells were collected by centrifugation at 7438 g for 8 min at 277 K. Protein purification steps were based on previously published purification protocols for MamAΔ41 from *Magnetospirillum magneticum* AMB-1 and *Magnetospirillum gryphiswaldense* MSR-1 [11,19–21]. In short, MamAΔ41-expressing cells were resuspended in buffer A (50 mM HEPES pH 7.5, 0.5 M NaCl, 20 mM imidazole and 5 mM βME) with the addition of DNase I (10 mg ml⁻¹) and a cocktail of protease inhibitors (100 μM phenylmethylsulfonyl fluoride (PMSF), 1.2 μg ml⁻¹ leupeptin and 1 μM pepstatin A). Cell disruption was performed by two cycles of French press pressure cell at 172 MPa and the soluble protein fraction was differentiated by centrifugation at 45,000 g for 90 min at 277 K. The soluble fraction was applied onto a home-made Ni-NTA column (HisPur Ni-NTA resin, Thermo scientific) pre-equilibrated against buffer A. Subsequent to protein binding, the column was step-washed by 50 ml of buffer B (20 mM HEPES pH 7.5, 1 M NaCl, 40 mM imidazole and 5 mM βME), 50 ml of buffer C (20 mM HEPES pH 7.5, 0.5 M NaCl, 40 mM imidazole and 5 mM βME) and eluted by buffer D (20 mM HEPES pH 7.5, 0.5 M NaCl, 0.5 M imidazole and 5 mM βME). The eluted protein was dialysed against buffer E (10 mM HEPES pH 7.5, 0.5 M NaCl and 5 mM βME) for 12 hours at 277 K followed by concentration using an Amicon Ultracel (3 kDa cutoff, Millipore), to a final volume of 2.5 ml. Concentrated protein was applied onto a size-exclusion column (Superdex 200, GE Healthcare Biosciences) pre-equilibrated with buffer E. Relevant protein peaks were merged, concentrated and flash frozen in liquid nitrogen and stored at 193 K for crystallisation trials. The ARSTM peaks that corresponded to monomeric and octameric protein forms were concentrated separately to 36 mg ml⁻¹ and 28 mg ml⁻¹, respectively.

Site-directed mutagenesis by PCR

The triple mutant (ARSTM) was generated using QuikChange site-directed mutagenesis (Stratagene). Coding and anti-sense primers containing a single mutagenic site were used for PCR amplification.

Crystallisation and diffraction collection

Crystallisation trials of ARSTM were conducted using the sitting-drop vapour-diffusion method. Initial screenings were performed using commercial screening kits obtained from Molecular Dimensions (Structure screen) and Hampton Research (Index screen) at 286 K and 277 K. Each drop contained a mixture of 0.2 μl of sampled reservoir and 0.2 μl of monomeric protein solution (28 mg ml⁻¹). Crystal harvesting was performed from optimised conditions of 0.1 M Tris pH 8.1, 0.75 M sodium potassium tartrate and 0.5% polyethylene glycol mono-methyl ether 5000. The crystals were then soaked for 5 seconds in a drop containing the same conditions, as well as 40% glycerol, serving as a cryo-protectant agent. Glycerol-protected crystals were then flash-cooled in liquid nitrogen. Diffraction dataset was collected on beamline ID14-4 at the European Synchrotron Radiation Facility (ESRF), Grenoble, France. Data was measured at the 0.939 Å wavelength for 230 images at an oscillation range of 0.65°, an exposure time of 0.375 sec per image and a crystal-to-detector distance of 422.81 nm. Data were reduced

and scaled using the HKL2000 program suite [28]. Phase acquisitions and structure determinations were performed using *BALBES: a molecular replacement pipeline* [29] followed by auto-build cycles using ARP/wARP [30]. The final model was built by Coot and refined in REFMAC5 [31]. For Rfree calculation, 5% of the data were excluded from both data sets. Structural figures were prepared using PyMOL [32] and Coot.

Least-squares overlaps

R.M.S. calculations were performed with SwissPDB viewer [33] using the domain alternate fit on C α to align structures on the basis of the conserved domain and to define the conformational changes of the structural homologues.

Electrostatic potential calculation

Calculations were performed in PyMOL using the adaptive Poisson-Boltzman solver (APBS) plug-in [34].

Circular dichroism (CD) analysis

CD measurements were conducted with a J750 Spectropolarimeter (Jasco, Mary's Court, Easton, USA) equipped with a Pelletier device. MamA protein samples were pre-diluted to 0.15 mg ml⁻¹ in buffer containing 150 mM NaCl, 10 mM Tris-HCl, pH 8, and measured with a 0.1 cm optical path suprasil quartz cuvette (Hellma, Müllheim, Germany). Thermal denaturation experiments of both samples were conducted by monitoring the dichroic absorption at 222 nm as a function of increased temperature varying from 25 to 90°C at a heating rate of 2.0°C·min⁻¹. Thermodynamic parameters associated with the temperature-induced denaturation of the protein were obtained by nonlinear, least-squares analysis of the temperature dependence of the CD spectrum.

Multiple sequence alignment and generation of phylogenetic trees

Initial multiple alignments were generated using the CLUSTAL W multiple alignment accessory application in the BioEdit sequence alignment editor [35]. Alignment was visualized using Jalview package [36]. Evolutionary trees were obtained using the MEGA 6 package [37] applying the Maximum Likelihood algorithm [38]. Bootstrap values were calculated with 100 replicates.

MamA protein sequences

All MamA sequences were obtained from GenBank. All accession numbers are shown in the phylogenetic tree in Fig 1.

Coordinates

Structure and structure factors have been submitted to the Protein Data Bank (accession codes: 4XI0).

Supporting Information

S1 Fig. Oligomeric state of purified MamA Δ 41 according to size exclusion (Superdex 200) chromatograms from different species. Elution profiles of MamA Δ 41 triple mutant from *Desulfovibrio magneticus* (RS-1) and wild type MamA Δ 41 from *Desulfovibrio magneticus* (RS-1), *M. magneticum* (AMB-1), *M. gryphiswaldense* (MSR-1) and *Candidatus Magnetobacterium*

bavaricum (Mbav) colored in light blue, green, red, orange and blue, respectively. Wild type MamA Δ 41 from RS-1 eluted in a volume corresponds to octamer (~192 kDa) whereas the triple mutated MamA Δ 41 eluted in three separate peaks that correspond to a 13-monomer oligomer (~312 kDa), octamer (~192 kDa) and a monomer (~24 kDa). Both MamA Δ 41 from AMB-1 and Mbav eluted at a volume corresponding to the monomer (20–22 kDa). MamA Δ 41 from MSR-1 eluted at a volume typical of the trimer (~60 kDa). Dashed green line represents the elution profile of protein markers: Ferritin (~440 kDa), Ovalbumin (~43 kDa), Carbonic Anhydrase (~29 kDa), Ribonuclease (~14 kDa).
(DOCX)

S2 Fig. Multiple sequence alignment of all 21 complete available MamA sequences from cultivated and uncultivated magnetotactic bacteria for which the 16S rRNA gene sequence is known. The MTB from *Alphaproteobacteria* class used in the analyses are: *Magnetospirillum magnetotacticum* (strain MS-1), *Ms. magneticum* (AMB-1), *Ms. gryphiswaldense* (MSR-1), strain SO-1, strain LM-1, *Magnetovibrio blakemorei* (MV-1), *Magnetospira* sp. QH-2, strain MO-1, *Magnetofaba australis* (IT-1) and *Magnetococcus marinus* (MC-1). Strain SS-5 from the *Gammaproteobacteria* class is also used. From the *Deltaproteobacteria* class MTB used include the magnetotactic multicellular prokaryotes *Ca. Magnetoglobus multicellularis* (MMP) and strain HK-1, *Ca. Desulfamplus magnetomortis* (BW-1), *Desulfovibrio magneticus* (RS-1 and FH-1), and strain ML-1. *Ca. Magnetobacterium bavaricum* (Mbav) and strain MYR-1 of the *Nitrospirae* phylum was also used. Red numbers at the bottom denote residue numbers specific for ArsTM.
(DOCX)

S3 Fig. Crystal contacts between two ArsTM monomers. The triple mutated residues (E140A, K141A and E143A, highlighted as red spheres in the top view) are found in the centers of these interaction surfaces.
(DOCX)

S4 Fig. Surface charge comparison of MamA Δ 41 structures. Surface charge comparison of MamA Δ 41 structures, with blue and red colours representing regions of positive and negative electrostatic potential, respectively. The molecule is shown in three views, namely the concave surface, a side view and the convex surface, related by 90° rotations. The surface charge representation of ArsTM and MamA Δ 41Mbav display a concave surface that is mainly positive and a convex surface that contains both positive and negative patches. The surface charge representation of MamA Δ 41AMB-1 displays a concave surface that is extremely positive and a mainly negative convex surface. All electrostatic surfaces representations were produced with the APBS plug-in of PyMOL under the same contour levels.
(DOCX)

S1 Table. MamA Δ 41 structure: Ramachandran statistics and missing residues.
(DOCX)

S2 Table. RMSD values of MamA Δ 41 monomers from alternative species compared against ArsTM.
(DOCX)

Acknowledgments

We would like to thank Dr Arash Komeili (UC Berkeley) for providing the *Desulfovibrio magneticus* RS-1 cells, Dr Long-Fei Wu (CNRS-LBC, France) for assistance with MamA sequences,

and the staff at ID14-4, ESRF (Grenoble, France) for their assistance during data collection. This research was made possible through grants from the Israeli Ministry of Science, Technology and Space and EMBO, the European Molecular Biology Organisation.

Author Contributions

Conceived and designed the experiments: NZ SC RZ. Performed the experiments: NZ SC CTL DB ZS GD. Analyzed the data: NZ SC CTL RZ. Contributed reagents/materials/analysis tools: CTL PA. Wrote the paper: NZ SC CTL RZ.

References

1. Lower BH, Bazylinski DA. The bacterial magnetosome: a unique prokaryotic organelle. *J Mol Microbiol Biotechnol.* 2013 Jan; 23(1–2):63–80 doi: [10.1159/000346543](https://doi.org/10.1159/000346543) PMID: [23615196](https://pubmed.ncbi.nlm.nih.gov/23615196/)
2. Pósfai M, Moskowitz BM, Arató B, Schüller D, Flies C, Bazylinski DA, et al. Properties of intracellular magnetite crystals produced by *Desulfovibrio magneticus* strain RS-1. *Earth Planet Sci Lett.* 2006 Sep; 249(3–4):444–55
3. Blakemore R. Magnetotactic bacteria. *Science* (80 -). 1975; 190:377–9
4. Lefèvre CT, Bazylinski DA. Ecology, diversity, and evolution of magnetotactic bacteria. *Microbiol Mol Biol Rev.* 2013; 77:497–526 doi: [10.1128/MMBR.00021-13](https://doi.org/10.1128/MMBR.00021-13) PMID: [24006473](https://pubmed.ncbi.nlm.nih.gov/24006473/)
5. Delong EF, Frankel RB, Bazylinski DA. Multiple evolutionary origins of magnetotaxis in bacteria. *Science.* 1993; 259:803–6 PMID: [17809345](https://pubmed.ncbi.nlm.nih.gov/17809345/)
6. Sakaguchi T, Burgess JG, Matsunaga T. Magnetite formation by a sulphate-reducing bacterium. *Nature.* 1993. p. 47–9
7. Flies CBCB, Peplies J, Schüller D. Combined approach for characterization of uncultivated magnetotactic bacteria from various aquatic environments. *Appl Environ Microbiol.* 2005; 71:2723–31 PMID: [15870364](https://pubmed.ncbi.nlm.nih.gov/15870364/)
8. Lefèvre CT, Vioria N, Schmidt ML, Pósfai M, Frankel RB, Bazylinski DA. Novel magnetite-producing magnetotactic bacteria belonging to the Gammaproteobacteria. *The ISME Journal.* 2012. p. 440–50
9. Kolinko S, Jogler C, Katzmann E, Wanner G, Peplies J, Schüller D. Single-cell analysis reveals a novel uncultivated magnetotactic bacterium within the candidate division OP3. *Environ Microbiol.* 2012; 14:1709–21 doi: [10.1111/j.1462-2920.2011.02609.x](https://doi.org/10.1111/j.1462-2920.2011.02609.x) PMID: [22003954](https://pubmed.ncbi.nlm.nih.gov/22003954/)
10. Sakaguchi T, Arakaki A, Matsunaga T. *Desulfovibrio magneticus* sp. nov., a novel sulfate-reducing bacterium that produces intracellular single-domain-sized magnetite particles. *Int J Syst Evol Microbiol.* 2002; 52:215–21 PMID: [11837306](https://pubmed.ncbi.nlm.nih.gov/11837306/)
11. Zeytuni N, Baran D, Davidov G, Zarivach R. Inter-phylum structural conservation of the magnetosome-associated TPR-containing protein, MamA. *J Struct Biol.* Elsevier Inc.; 2012 Dec; 180(3):479–87 doi: [10.1016/j.jsb.2012.08.001](https://doi.org/10.1016/j.jsb.2012.08.001) PMID: [22917855](https://pubmed.ncbi.nlm.nih.gov/22917855/)
12. Lefèvre CT, Wu LF. Evolution of the bacterial organelle responsible for magnetotaxis. *Trends in Microbiology.* 2013. p. 534–43
13. Lefèvre C, Trubitsyn D, Abreu F, Kolinko S, de Almeida LGP, de Vasconcelos ATR, et al. Monophyletic origin of magnetotaxis and the first magnetosomes. *Environ Microbiol.* 2013 Aug; 15(8):2267–74 doi: [10.1111/1462-2920.12097](https://doi.org/10.1111/1462-2920.12097) PMID: [23438345](https://pubmed.ncbi.nlm.nih.gov/23438345/)
14. Komeili A, Vali H, Beveridge TJ, Newman DK. Magnetosome vesicles are present before magnetite formation, and MamA is required for their activation. *Proc Natl Acad Sci U S A.* 2004; 101:3839–44 PMID: [15004275](https://pubmed.ncbi.nlm.nih.gov/15004275/)
15. Murat D, Quinlan A, Vali H, Komeili A. Comprehensive genetic dissection of the magnetosome gene island reveals the step-wise assembly of a prokaryotic organelle. *Proc Natl Acad Sci U S A.* 2010 Mar 23; 107(12):5593–8 doi: [10.1073/pnas.0914439107](https://doi.org/10.1073/pnas.0914439107) PMID: [20212111](https://pubmed.ncbi.nlm.nih.gov/20212111/)
16. Nakazawa H, Arakaki A, Narita-Yamada S, Yashiro I, Jinno K, Aoki N, et al. Whole genome sequence of *Desulfovibrio magneticus* strain RS-1 revealed common gene clusters in magnetotactic bacteria. *Genome Res.* 2009 Oct; 19(10):1801–8 doi: [10.1101/gr.088906.108](https://doi.org/10.1101/gr.088906.108) PMID: [19675025](https://pubmed.ncbi.nlm.nih.gov/19675025/)
17. Lefèvre CT, Trubitsyn D, Abreu F, Kolinko S, Jogler C, de Almeida LGP, et al. Comparative genomic analysis of magnetotactic bacteria from the Deltaproteobacteria provides new insights into magnetite and greigite magnetosome genes required for magnetotaxis. *Environ Microbiol.* 2013; 15:2712–35 doi: [10.1111/1462-2920.12128](https://doi.org/10.1111/1462-2920.12128) PMID: [23607663](https://pubmed.ncbi.nlm.nih.gov/23607663/)

18. Yamamoto D, Taoka A, Uchihashi T, Sasaki H, Watanabe H, Ando T, et al. Visualization and structural analysis of the bacterial magnetic organelle magnetosome using atomic force microscopy. *Proc Natl Acad Sci U S A*. 2010; 107:9382–7 doi: [10.1073/pnas.1001870107](https://doi.org/10.1073/pnas.1001870107) PMID: [20439702](https://pubmed.ncbi.nlm.nih.gov/20439702/)
19. Zeytuni N, Ozyamak E, Ben-Harush K, Davidov G, Levin M, Gat Y, et al. Self-recognition mechanism of MamA, a magnetosome-associated TPR-containing protein, promotes complex assembly. *Proc Natl Acad Sci*. 2011; 108(33):E480–7 doi: [10.1073/pnas.1103367108](https://doi.org/10.1073/pnas.1103367108) PMID: [21784982](https://pubmed.ncbi.nlm.nih.gov/21784982/)
20. Zeytuni N, Zarivach R. Crystallization and preliminary crystallographic analysis of the *Magnetospirillum magneticum* AMB-1 and *M. gryphiswaldense* MSR-1 magnetosome-associated proteins MamA. *Acta Crystallogr Sect F Struct Biol Cryst Commun*. International Union of Crystallography; 2010 Jul 1; 66(Pt 7):824–7
21. Zeytuni N, Zarivach R. Purification of the *M. magneticum* strain AMB-1 magnetosome associated protein MamADelta41. *J Vis Exp*. 2010 Jan;(37):):8–12
22. Baud F, Karlin S. Measures of residue density in protein structures. *Proc Natl Acad Sci U S A*. 1999; 96:12494–9. PMID: [10535950](https://pubmed.ncbi.nlm.nih.gov/10535950/)
23. Conte L Lo, Chothia C, Janin J, Lo Conte L. The atomic structure of protein-protein recognition sites. *J Mol Biol*. 1999; 285:2177–98. Available: <http://dx.doi.org/10.1006/jmbi.1998.2439> PMID: [9925793](https://pubmed.ncbi.nlm.nih.gov/9925793/)
24. Goldschmidt L, Cooper DR, Derewenda ZS, Eisenberg D. Toward rational protein crystallization: A Web server for the design of crystallizable protein variants. *Protein Sci*. 2007; 16:1569–76 PMID: [17656576](https://pubmed.ncbi.nlm.nih.gov/17656576/)
25. Ashkenazy H, Erez E, Martz E, Pupko T, Ben-Tal N. ConSurf 2010: Calculating evolutionary conservation in sequence and structure of proteins and nucleic acids. *Nucleic Acids Res*. 2010;38
26. Celniker G, Nimrod G, Ashkenazy H, Glaser F, Martz E, Mayrose I, et al. ConSurf: Using evolutionary data to raise testable hypotheses about protein function. *Israel Journal of Chemistry*. 2013. p. 199–206
27. Studier FW. Protein production by auto-induction in high-density shaking cultures. *Protein Expression and Purification*. 2005. p. 207–34
28. Otwinowski Z, Minor W. Processing of X-ray diffraction data collected in oscillation mode. *Methods Enzymol*. 1997; 276:307–26
29. Long F, Vagin AA, Young P, Murshudov GN. BALBES: A molecular-replacement pipeline. *Acta Crystallographica Section D: Biological Crystallography*. 2007. p. 125–32
30. Cohen SX, Ben Jelloul M, Long F, Vagin A, Knipscheer P, Lebbink J, et al. ARP/wARP and molecular replacement: The next generation. *Acta Crystallographica Section D: Biological Crystallography*. 2007. p. 49–60
31. Vagin AA, Steiner RA, Lebedev AA, Potterton L, McNicholas S, Long F, et al. REFMAC5 dictionary: organization of prior chemical knowledge and guidelines for its use. *Acta Crystallogr Sect D Biol Crystallogr*. International Union of Crystallography; 2004 Dec; 60(Pt 12 Pt 1):2184–95
32. DeLano WL. The PyMOL Molecular Graphics System. Schrödinger LLC www.pymol.org. 2002;Version 1. Available: <http://www.pymol.org>
33. Guex N, Peitsch MC. SWISS-MODEL and the Swiss-PdbViewer: An environment for comparative protein modeling. *Electrophoresis*. 1997; 18:2714–23 PMID: [9504803](https://pubmed.ncbi.nlm.nih.gov/9504803/)
34. Baker NA, Sept D, Joseph S, Holst MJ, McCammon JA. Electrostatics of nanosystems: application to microtubules and the ribosome. *Proc Natl Acad Sci U S A*. 2001; 98:10037–41 PMID: [11517324](https://pubmed.ncbi.nlm.nih.gov/11517324/)
35. Hall T. BioEdit: a user-friendly biological sequence alignment editor and analysis program for Windows 95/98/NT. *Nucleic Acids Symp Ser*. 1999; 41:95–8
36. Waterhouse AM, Procter JB, Martin DMA, Clamp M, Barton GJ. Jalview Version 2-A multiple sequence alignment editor and analysis workbench. *Bioinformatics*. 2009; 25:1189–91 doi: [10.1093/bioinformatics/btp033](https://doi.org/10.1093/bioinformatics/btp033) PMID: [19151095](https://pubmed.ncbi.nlm.nih.gov/19151095/)
37. Tamura K, Stecher G, Peterson D, Filipinski A, Kumar S. MEGA6: Molecular evolutionary genetics analysis version 6.0. *Mol Biol Evol*. 2013; 30:2725–9 doi: [10.1093/molbev/mst197](https://doi.org/10.1093/molbev/mst197) PMID: [24132122](https://pubmed.ncbi.nlm.nih.gov/24132122/)
38. Guindon S, Gascuel O. A simple, fast, and accurate algorithm to estimate large phylogenies by maximum likelihood. *Syst Biol*. 2003; 52:696–704 PMID: [14530136](https://pubmed.ncbi.nlm.nih.gov/14530136/)